Stratified continuum percolation: Scaling geometry of hierarchical cascades

D. D. Nolte
Department of Physics, Purdue University, West Lafayette, Indiana 47907

L. J. Pyrak-Nolte
Department of Earth and Atmospheric Science, Purdue University, West Lafayette, Indiana 47907

(Received 8 April 1991)

Stratified percolation patterns result from hierarchical cascades with continuous overlap. The pattern construction is a hybrid process, combining continuum percolation with random curdling. Stratified percolation is a correlated percolation with fractal dimensions that can be continuously tuned. The percolation threshold is found to vary with changing correlations. The density of percolating sites is approximately log-normal and can be described by a multifractal. Trends in the $f(\alpha)$ curves are studied as fractal dimensions are changed. The finite-size-scaling properties are investigated using Monte Carlo real-space renormalization. Because the patterns have features at all length scales, stratified percolation has intrinsically small-cell renormalization properties. However, the small-cell properties can be removed by transforming the occupation fraction into an equivalent occupancy for standard uncorrelated continuum percolation. The transformed threshold is approximately invariant with respect to changing correlations and is close to the standard value of $a_c = 0.7$ for isotropic continuum systems. Stratified percolation has a correlation length exponent of $\nu = 1.33 \pm 0.05$.

PACS number(s): 64.60.Ak, 05.50.+q, 05.70.Jk, 92.40.Kf

I. INTRODUCTION

Hierarchical cascades represent sequences of probabilities. A wide range of physical systems arise from random cascades, as features on smaller scales evolve from features at larger scales. Examples range from the extreme macroscopic scale (such as clustering of galaxies) to the extreme microscopic scale (such as hadronization in high-energy particle collisions). The length scales of these examples span more than 50 orders of magnitude. If the successive steps possess self-similarity of some degree, then the cascade leads to fractal structures. Structure at larger scales produces strong correlations at smaller scales.

Of interest in some cases are cascades in which features at larger scales overlap with features at smaller scales. Overlap mixes the effects at different scales, so that the processes at one scale are no longer independent of processes at other scales. Overlap converts the random cascade into a random process with multifractal scaling properties and an approximately log-normal distribution of densities. Two random Cantor bars are shown in Fig. 1, one without overlap, one with overlap. In both cases, $N = 3$ and the scale factor is $b = 4$. In the case of no overlap, the fractal dimension is $D = \ln 2 / \ln 4 = 0.79$. In the case with overlap, on the other hand, the fractal dimension is smaller than this value. The densities of the bar after three iterations are shown at the bottom of the figure. By allowing overlap, regions of very high density occur. The high density produces an extended tail on the mass distribution that is a signature of random multiplicative processes. The high density also influences multifractal properties that depend on mass moments. In this paper, we explore some of the consequences of hierarchical cascades with continuous overlap, and relate them to problems in correlated percolation. To illustrate the properties, we take a model called "stratified continuum percolation" as a specific example.

Stratified percolation is a correlated percolation model that generates fractal patterns through a self-similar cascade. Overlap of subcascades is allowed, leading to approximately log-normal densities. The model was initially developed to describe the geometry of flow paths in single fractures in rock [1], and was found to have many features that accurately reproduced experimental observations on fracture properties [2]. It was subsequently discovered to have a percolation threshold that is approx-

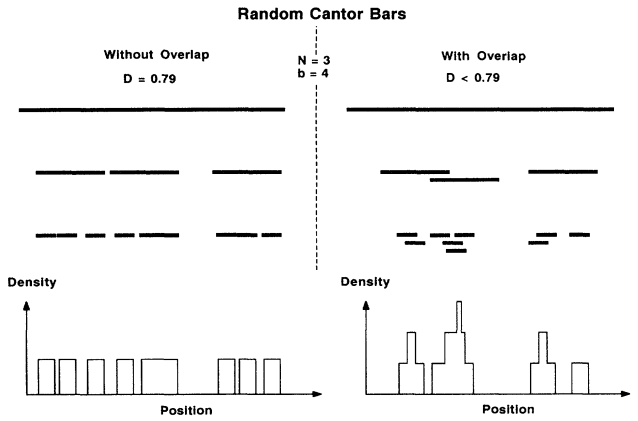

FIG. 1. Random Cantor bars with $N = 3$ and $b = 4$. Without overlap, the fractal dimension is $D = 0.79$. With overlap, the resulting mass distribution is multifractal.

imately invariant with respect to changing correlations [3]. This model is part of a larger class of correlated percolation systems, in which occupancy is conditionally dependent on local environments.

Much of correlated percolation has been motivated through Ising percolation. Ising clusters in two dimensions (2D) comprise equilibrium systems with near-neighbor exchange interactions and long-range correlations near T_c. The connectivity of clusters in the Ising model has been related to the geometric critical behavior of percolation systems [4–9]. In addition to equilibrium Ising percolation, other correlated percolation systems have also been studied. These systems include irreversible cooperative filling [10–13], restricted valence [14,15], Voter models [16], and other correlated percolation models [17–19]. Some general properties of correlated percolation have been addressed [20], but systematic study of correlated percolation has been difficult because of the wide variety of possible correlations that can occur naturally in experimental systems, or in model simulations.

Much of continuum percolation theory [21–24] is based on random continuum percolation. A continuum percolation pattern is shown in Fig. 2(a). Squares are randomly positioned within the region of interest. This pattern is close to the percolation threshold, with 60% of the figure covered by the squares. A continuum cluster spans the pattern. This "critical" cluster is shown in Fig. 2(b). The fractal dimension of the critical cluster is $D=1.89$, although the pattern including all covered positions in Fig. 2(a) has $D=2.00$.

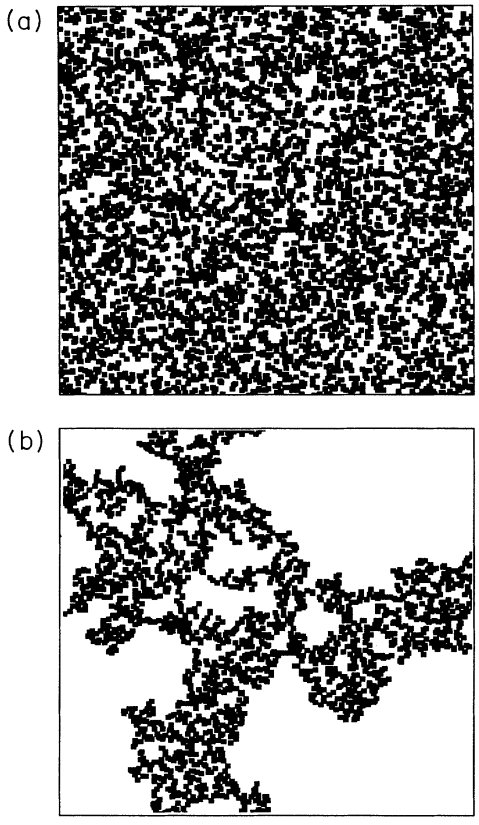

FIG. 2. Standard continuum percolation pattern near the percolation threshold. The full pattern is shown in (a). The pattern has 5000 squares plotted randomly. The total area fraction covered is 60%. The critical cluster is shown in (b).

The random pattern in Fig. 2 fails to reproduce the correlated structure observed in many natural systems. A natural percolation system is shown in Fig. 3. The black pattern is the void space inside a fracture in Monzonite granite rock [25]. The white areas are the areas of contact between the fracture surfaces. The photograph, showing a region 4 mm by 2 mm in size, was obtained by making a metal cast of the fracture. The metal fills the void spaces between the fracture surfaces and represents the possible flow routes of a fluid percolating through the fracture. The pattern has spatial correlation. Void spaces and contact area are separately clumped. It has similar structures on many length scales and has a fractal dimension of $D=1.94$. The area covered by metal (the flow paths) is 62%. The strong correlations present in the pattern in Fig. 3 may be expected to have altered the critical threshold. This shift of critical thresholds is a characteristic property of correlated percolation systems [26]. Different degrees of correlation will lead to different critical thresholds. When confronted with experimental data, such as in Fig. 3, the primary question is how far this system is away from the critical threshold. In the presence of the correlations, it is not immediately clear what the answer to this question will be.

In this paper we address these questions, and describe stratified percolation, which produces strongly correlat-

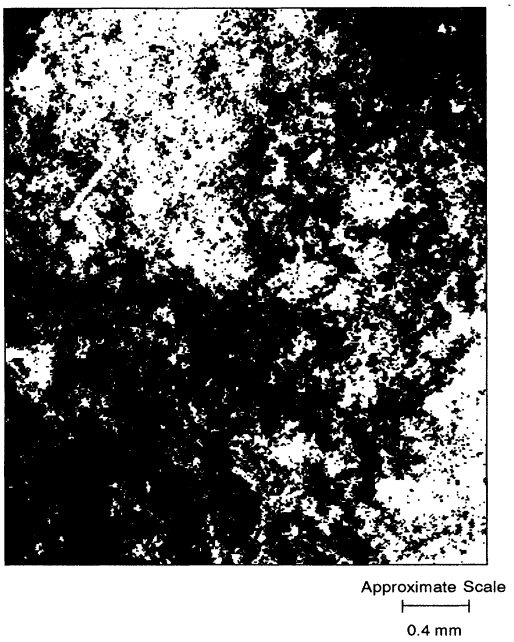

FIG. 3. Scanning electron micrograph of a metal cast of the flow paths in a fracture in granite rock. The pattern covers an area 4×2 mm^2. The black regions are the metal. The pattern shows features at all length scales and has a fractal dimension $D=1.94$.

ed, fractal percolation structures. In Sec. II we describe the overlapping cascade algorithm that generates the stratified patterns. The construction can be viewed as a hybrid between continuum percolation and random curdling. In Sec. III the classical geometrical properties of the patterns are presented. The covered area and site density are discussed. In Sec. IV the fractal structure of stratified percolation is developed, including lacunarity and multifractal properties of the site density. The percolation properties are investigated in Sec. V using Monte Carlo real-space-renormalization techniques to obtain percolation thresholds and the correlation length exponent.

II. STRATIFIED PERCOLATION PATTERN FORMATION

Stratified percolation patterns are generated by a recursive algorithm that defines a self-similar cascade of random sites [27]. A demonstration of the algorithm is shown in Fig. 4. The construction may be regarded as applying random continuum percolation on successively smaller scales. The figure contains three scales, or tiers, that are related by a scale factor b, where $b=4$ in the figure. In the first tier, or largest square, N sites are randomly placed. The N second squares are squares with a linear size reduced by the factor b from the size of the larger square. The algorithm repeats, now randomly placing N sites in each of the N second tier squares. The final black squares are plotted within the third tier. In Fig. 4, $N=5$ and there are $M=5^3=125$ final squares.

The recursive algorithm is expressed as

$$\begin{aligned} s_{i,n} &= s_{j,n-1} + b^{1-n}(r_1, r_2) \\ &\vdots \\ s_{1,0} &= (0,0)\ , \end{aligned} \tag{2.1}$$

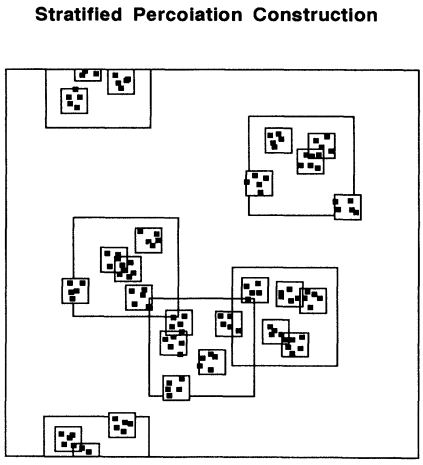

FIG. 4. Recursive construction of a stratified percolation pattern. The figure includes three tiers with a scale factor of $b=4$ between tiers. There are five squares plotted randomly at each sublevel ending with a total $5^3=125$ squares plotted. The cascade structure is clearly evident and introduces strong correlations in the placement of the smallest squares.

where $s_{i,n}$ is a two-component vector giving the x and y coordinates of the new site, r_1 and r_2 are uniformly distributed random numbers between 1 and -1, and i is the ith site on the nth tier inside a square region around the jth site of the $(n-1)$th tier. The total number of final (smallest) squares plotted is N^n, where N is the number of squares per tier, and n is the number of tiers. The first tier is centered at the origin. During the construction, some final points land outside of the largest sample region. We apply wraparound boundary conditions so that these points are plotted within the sample region inside the opposite boundary. This boundary condition is demonstrated in Fig. 4. This wraparound is applied only on the largest tier. For smaller tiers, points are allowed to overhang the smaller sample regions.

The stratified percolation construction is intrinsically a continuum construction. At each scale, the subsquares are centered randomly within the next larger tier, such that each tier is a continuum percolation plot of its own. Even at the smallest level, when the final squares are plotted, the squares are placed randomly as a continuum plot. In practice, however, the final squares are plotted into a grid. In our simulations, the grid is 300×300 pixels. The final squares are $m\times m$ pixels, and therefore are not strictly plotted continuously within the regions. If m is large, then the continuum limit is satisfied. If m is small, then the discreteness of the underlying grid will begin to affect percolation thresholds. In particular, if $m=1$, then the pattern is in the limit of a correlated lattice percolation system, which has a different threshold than the continuum case. For our simulations, we choose the scale factor b and the number of tiers so that a final square size is 4×4 pixels. This choice allows us to retain all the essential features of continuum percolation. This size of the smallest squares in the cascade determines the lower cutoff for the scaling properties of the patterns.

Examples of stratified percolation patterns are shown in Fig. 5 for different numbers of tiers, scale factors, and the number of points per tier. Figure 5(a) has three tiers, a scale factor of $b=4.22$ and $N=22$ points per tier. Figure 5(b) has five tiers, $b=2.37$ and $N=7$. These patterns exhibit the strong correlations seen in Fig. 3 that were missing from the uncorrelated percolation construction in Fig. 2. Both Figs. 5(a) and 5(b) are near the percolation threshold. The fractions of area that are covered are 59% and 65%, respectively. These area fractions are lower than the threshold $p_c=0.7$ for conventional continuum percolation. The clumped structures introduced by the cascade algorithm enhance the probability of percolation. More of the continuum percolation properties will be discussed in a later section. A stratified site percolation pattern below the threshold is shown in Fig. 5(c). The site percolation properties will not be discussed in this paper.

Stratified percolation has much in common with curdling. Curdling is a process whereby an originally uniform mass clumps together into many small regions with high density [27]. Curdling processes, especially self-similar processes, involve a cascade in which the mass sequentially breaks into smaller subsets of larger subsets. Many models involving curdling have been developed.

Some older models include scaling models of the mass distribution in galaxies and the universe [28,29]. The production of turbulent structures in which the spatial distribution is generated by a cascade was also modeled [30]. Multifractal lattices have been generated through cascade processes [31,32]. The cascade in stratified percolation is obvious, leading also to a curdled structure.

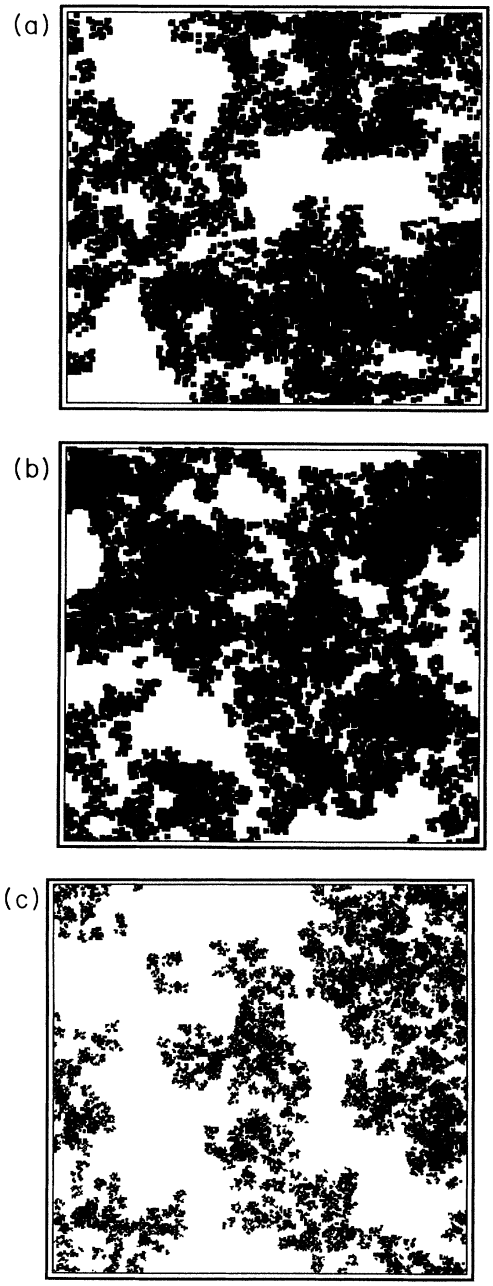

FIG. 5. Examples of stratified percolation patterns with $m=4$ for (a) three tiers with $b=4.22$ and $N=22$ with $D=1.95$ and $A=0.59$; (b) five tiers with $b=2.37$ and $N=7$ with $D=1.97$ and $A=0.65$; and (c) five tiers with $b=3.13$ and $N=10$ with $D=1.89$ and $A=0.29$. (c) is a correlated lattice percolation pattern with $m=1$.

III. STRATIFIED PERCOLATION PATTERN STRUCTURE

A. Covered area

The covered area of a percolation pattern is one of the key parameters used to characterize the system. The critical threshold is usually expressed as a critical covered area. For random (uncorrelated) continuum percolation, a simple expression relates the covered area to the number and size of blocks written in the pattern. For a number N of small blocks with area l^2, distributed within a large area L^2, the covered area is given by

$$a=(1-e^{-N(l/L)^2}) . \tag{3.1}$$

The ratio $N(l/L)^2$ can also be expressed as N/b^2, where b is the linear scale factor relating l to L. The area is therefore given by

$$a=(1-e^{-N/b^2}) . \tag{3.2}$$

In the stratified construction, the conventional continuum percolation construction is applied at each scale, or tier. We can therefore introduce a parameter $a(N)$ called the area fraction per tier, given approximately by Eq. (3.2) for large N. For patterns with many tiers, N can be relatively small. For instance, in Fig. 5(b) with five tiers, $N=7$. In the case of small N, the expression for covered area is obtained by finding the probability that a position is not covered after N squares are plotted. The probability P_1 that a position is *not* covered after one square is plotted is

$$P_1=1-1/b^2 .$$

The probability P_2 that it is not covered after two squares are plotted is given by the product of the probability that it is not covered by the first square with the probability that it is not covered by the second square because the probabilities are independent. This is

$$P_2=(1-1/b^2)(1-1/b^2)=(1-1/b^2)^2 .$$

By extension, the area that remains uncovered (white) after N squares are plotted is equal to $(1-1/b^2)^N$. Therefore the area covered (black) is

$$a(N,b)=1-(1-1/b^2)^N . \tag{3.3}$$

This expression gives the area covered by each tier in the stratified construction, where N blocks are plotted in the sample region. The area fraction per tier is a convenient parameter to help classify the structure of stratified percolation. We shall see in a later section that the percolation properties of stratified percolation are naturally expressed in terms of the area fraction per tier.

The total area of a stratified percolation pattern is obtained recursively from the area fraction per tier. For one tier, the area fraction is $A(1,N)=a(N,b)$. For two tiers the covered area is $A(2,N)=1-[1-A(1,N)/b^2]^N$, because the plotted squares are now composed by the first tier. By extension, the recursive expression for the total covered area of a stratified pattern for n tiers and N squares is

$$A(n,N)=1-[1-A(n-1,N)/b^2]^N$$
$$\vdots \qquad (3.4)$$
$$A(1,N)=a(N,b)\ .$$

Equation (3.4) would be exact if wraparound boundary conditions were applied on each tier, i.e., if squares were not plotted outside the bounds of the smaller tiers. In our construction, we apply wraparound boundary conditions only for the largest tier. Equation (3.4) is therefore approximate, and underestimates the true area fraction. The total area fraction for five tiers with $b=2.37$ is plotted in Fig. 6 as a function of the area fraction per tier for N varying from 4 to 11. The data are obtained from Monte Carlo simulations, and are compared with Eq. (3.4).

B. Density distribution

The patterns in Fig. 5 are two dimensional; positions are either covered or not. A third degree of freedom can be gained by considering the density of covered positions. The density of sites is obtained during the plotting of the pattern by counting the number of times that a given position is covered by a plotted square. The density of sites for a five-tier pattern with $N=10$ and $b=2.37$ is displayed in Fig. 7. The white areas represent zero density; the shades of gray of increasing darkness represent increasingly larger density of sites. The correlations introduced during the cascade algorithm are clearly visible. Regions of high density and low density are separately clumped. The distribution of site densities is shown in Fig. 8. The frequency of occurrence of a specific density is plotted as a function of site density. The probability density is not Gaussian, and is approximately log-normal. Log-normal distributions are characteristic of hierarchical models [33,34]. The long tail of high densities is caused during the cascade construction as many squares overlap with one another. It is interesting to note that the density of sites can be equated with distributions of apertures for a fluid-flow network [2]. The long tail of large "apertures" has been found to be particularly relevant for aperture distributions in fractures in rock [35–37].

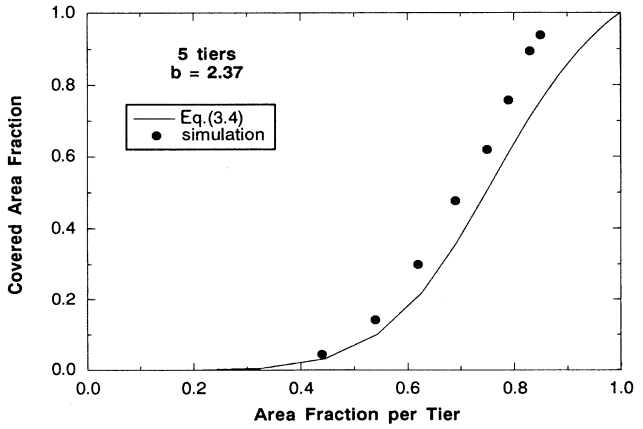

FIG. 6. The total area covered by the stratified pattern as functions of the area covered per tier for five tiers with $b=2.37$ for varying $N=4$ to 11. The data points are from simulations. The lack of wraparound boundary conditions on the smaller tiers creates a significant deviation from the values predicted by Eq. (3.4).

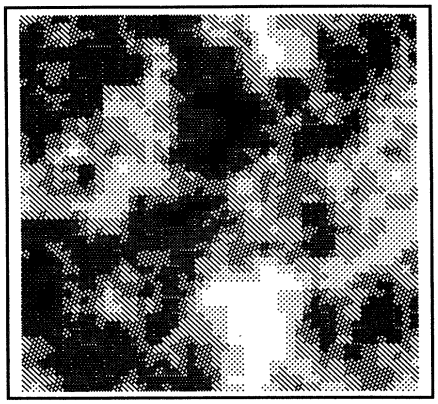

FIG. 7. Density of sites for a five-tier pattern with $b=2.37$ and $N=10$. Increasing shades of gray denote increasing densities. The density of sites is strongly correlated, reflecting the overlapping cascade construction processes.

IV. FRACTAL STRUCTURE

The stratified percolation patterns are fractal within the limits of the upper and lower cutoff lengths. The upper cutoff length is the initial sample size, and the small cutoff length is the size of the final squares. Within these limits, the black-and-white patterns are scale invariant and are characterized by a fractal dimension. The degree of homogeneity of the two-dimensional patterns is characterized using lacunarity. When the density of sites is considered, the patterns are multifractal and exhibit a distribution of fractal dimensions and Lipschitz-Hölder

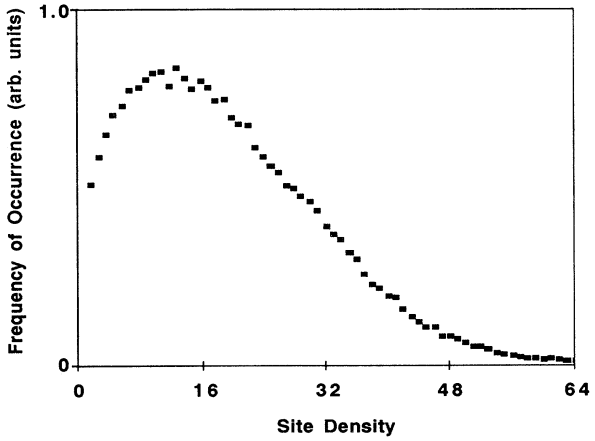

FIG. 8. Distribution of the site density for Fig. 7 showing the frequency of occurrence for different densities. The distribution has a long tail of large densities that is approximately described by a log-normal distribution.

exponents. All of these aspects of the stratified patterns are discussed in this section. The two-dimensional properties are discussed first, followed by the multifractal analysis.

A. Fractal dimension

The fractal dimension of the full stratified patterns (i.e., not just the spanning clusters) can be estimated by considering the cascade construction of the patterns. The fractal dimension is obtained by counting the number of squares that will cover the pattern for a specific square edge length. On the first tier, the fraction of the area that is covered by the covering squares is just $a(N)$, the area fraction per tier, given by Eq. (3.3). On the second tier, if squares did not overlap, then the fraction of the area covered would be $a(N)^2$, i.e., the product of the area fractions. In the construction, however, overlap does occur. The fraction of area that is overlapped by M squares is given by

$$a_M(N)=\frac{1}{M!}\sum_{i\neq j\neq\cdots}^{N}[a(1)]^M[1-a(N-M)]$$
$$=\frac{N!}{M!(N-M)!}[a(1)]^M[1-a(N-M)]\ , \quad (4.1)$$

where we have dropped the notation of $a(N,b)$ from Eq. (3.3) in favor of the shorthand notation $a(N)$ with a scale factor b implied. The overlap is the sum over all distinguishable permutations of the products of the probability $[a(1)]^M$ that a position is covered by M squares, by the probability $[1-a(N-M)]$ that it is *not* covered by the $N-M$ remaining squares. In the regions of overlap, covering a fraction $a_0(N)=\sum_{M=2}a_M(N)$ of the pattern, there is an enhanced density of small squares, obtaining contributions from each of the larger squares. This region consists of double overlaps, triple overlaps, etc. If the amount of double overlap is considerably larger than triple overlap, then the covering area fraction is approximately equal to the product $a_0(N)a(2N)$. The covering area fraction $A(n,N)$ for the nth tier is therefore approximately

$$A(1,N)=a(N)\ ,$$
$$A(2,N)=a(N)[a(N)-a_0(N)]+a_0(N)a(2N)$$
$$=a(N)\{a(N)[1-a(N-1)]+a(N-1)a(2N)\}$$
$$\vdots \quad (4.2)$$
$$A(n,N)=a(N)\{a(N)[1-a(N-1)]$$
$$+a(N-1)a(2N)\}^{n-1}\ ,$$

where the approximation

$$a_0(N)\approx a(N)a(N-1) \quad (4.3)$$

has been used in place of Eq. (4.1). We make this last approximation in order to extrapolate to the last line in Eq. (4.2). The error in this approximation is order $O(b^{-2})\approx 10\%$ on the value for the area fraction. However, the scaling of the area fraction from one tier to the next is preserved. Using these expressions, the fractal dimension is approximately given by

$$D\approx 2+\frac{(n-1)}{n}\frac{\ln\{a(N)[1-a(N-1)]+a(2N)a(N-1)\}}{\ln b}. \quad (4.4)$$

With one tier, $n=1$ and the fractal dimension is strictly $D=2.00$, as expected. The fractal dimensions of Eq. (4.4) are plotted as functions of $a(N)$ in Fig. 9 for five-tier patterns. The agreement with the simulations using the box-counting technique is good, confirming our use of the approximations mentioned above. The fractal dimensions are shown in Fig. 10 as functions of the total area fraction $A(N,b)$ for three-and five-tier simulations.

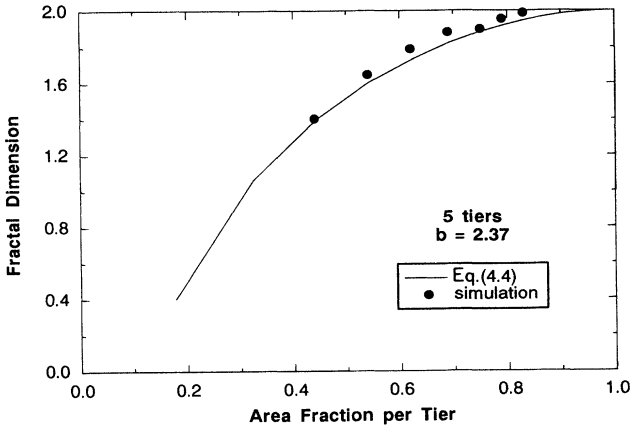

FIG. 9. Fractal dimension D vs the area per tier for five tiers. The data points are obtained from simulations and box counting by varying the number of points per tier $N=4$ to 10. The curve is from Eq. (4.4).

B. Lacunarity

Fractal patterns are not uniquely defined by their fractal dimension. The fractal dimension gives the size scal-

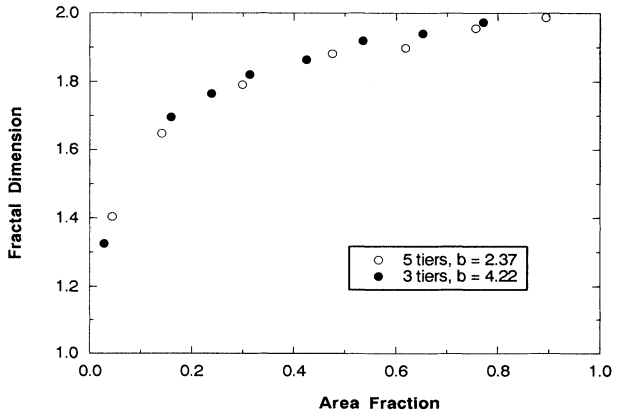

FIG. 10. The fractal dimension takes on an approximately universal behavior when it is plotted vs the total area of the patterns. The data are from simulations for three and five tiers with $b=4.22$ and 2.37, respectively.

ing behavior of the pattern, but does not describe how homogeneously the pattern is distributed. The term "lacunarity" was coined by Mandelbrot [27] to refer to the magnitude of the "gaps" in the pattern. One common definition of lacunarity $\Lambda(L)$ is the mean square deviation of the covered area fractions for a certain size L

$$\Lambda(L)=\frac{\langle A^2(L)\rangle-\langle A(L)\rangle^2}{\langle A(L)\rangle^2} \tag{4.5}$$

where $A(L)$ is the fraction of the area that is covered in a square of linear size L. Various schemes have been proposed to average $\Lambda(L)$ over L to obtain the lacunarity of a pattern [38–40]. We have altered the approach of Taguchi, by using a logarithmic weighting of the $\Lambda(L)$, rather than a linear weighting. A linear weighting will weight more heavily toward the large sizes. The average lacunarity Λ is

$$\Lambda=\frac{1}{n}\sum_{i=1}^{n}\Lambda(2^i)\ . \tag{4.6}$$

The measured lacunarities for Monte Carlo simulations of stratified percolation patterns with three tiers are given in Fig. 11 as a function of the measured area fraction. In Fig. 11, the lacunarity increases as the covered area fraction decreases. The lacunarity vanishes when $A=1.0$, because the pattern is completely homogeneous, i,e., is entirely covered. As the uncovered areas grow in size with reduced occupancy, the inhomogeneities in the pattern grow. The lacunarity diverges as the covered area vanishes, because the denominator in Eq. (4.5) vanishes faster than the fluctuations. The lacunarity gives only a limited description of the distribution of mass in a pattern. A much fuller description is given by considering the multifractal properties of the patterns.

C. Multifractal properties

Curdling processes have a natural connection with multifractal pattern formation. Multifractals were embedded in weight curdling [27,41], and were developed to characterize turbulence and strange attractors of deterministic chaotic systems [42–45]. Percolation systems were also found to consist of multifractal sets [46–48] when the bonds are assigned values proportional to the voltage drops across the bonds. Other systems also show multifractality, such as aggregation processes [31,49,50].

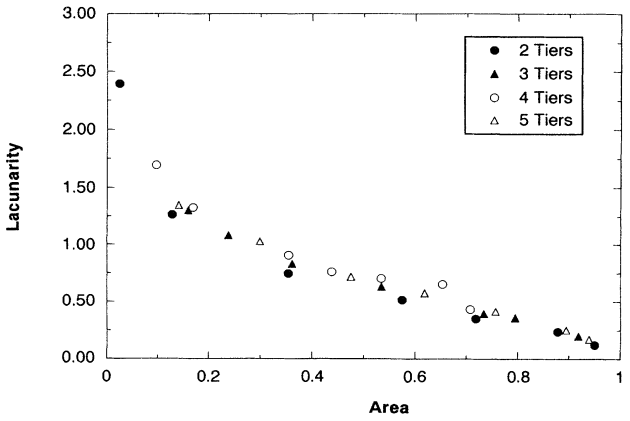

FIG. 11. The lacunarity takes on approximately universal behavior when plotted vs the total area of the patterns. The data in the figure are from simulations of 2–5 tiers.

A multifractal set S is the union of fractal subsets S_α,

$$S=US_\alpha\ ,$$

where α is a scaling exponent that describes the singularities of the S_α subset. This parameter α is called the Lipschitz-Hölder exponent. The mass μ_α in a cell of size L of the subset S_α varies as

$$\mu_\alpha \propto L^\alpha\ . \tag{4.7}$$

The subset S_α has a unique fractal dimension $f(\alpha)$ defined through the expression

$$\mathcal{N}(\alpha,L)d\alpha=\rho(\alpha)L^{-f(\alpha)}d\alpha \tag{4.8}$$

in which $\mathcal{N}(\alpha,L)d\alpha$ is the number of boxes of side L that are needed to cover sets S_α in the range of α to $\alpha+d\alpha$, where the density $\rho(\alpha)d\alpha$ is the number of sets from S_α to $S_{\alpha+d\alpha}$.

When confronted with an experimental pattern, it is not possible directly to isolate the subsets S_α and isolate the fractal dimensions. However, it is possible to cover the pattern with N cells with side of length L and count the total mass enclosed in the cell. A weight μ_i can be set equal to the total "mass" enclosed in the ith cell. An expression for $N(L)$ is obtained by raising μ_i to the power q. In this case the power q expresses the mass moment of the distribution of masses that define the pattern. The definition for the weighted number of boxes $N(q,L)$ is

$$N(q,L)=\sum_{i=1}^{N}\mu_i^q \propto L^{-\tau(q)}\ , \tag{4.9}$$

where the mass exponent $\tau(q)$ is given by

$$\tau(q)\approx-\frac{d\ \ln N(q,L)}{d\ \ln L}\ . \tag{4.10}$$

For the special case $q=0$, and only for this special case, the weighted number of boxes $N(q,L)$ reduces to the number of boxes needed to cover the pattern $N(L)$ yielding $\tau(q)=D$. Another special case is $q=1$, for which $\tau(q)=0$ because the masses are normalized to $\sum_i\mu_i=1$.

The connection between the mass exponent $\tau(q)$ and the fractal dimension that describes the qth mass moment of the pattern is given by the Legendre transformations

$$f(\alpha)=\tau(q)+\alpha q\ , \tag{4.11}$$

$$\alpha(q)=-\frac{d}{dq}\tau(q)\ . \tag{4.12}$$

Equations (4.11) and (4.12) make it possible to describe the fractal dimension $f(q)$ for varying q, or $f(\alpha)$ for varying α, based on the weighted number of boxes in Eq. (4.9).

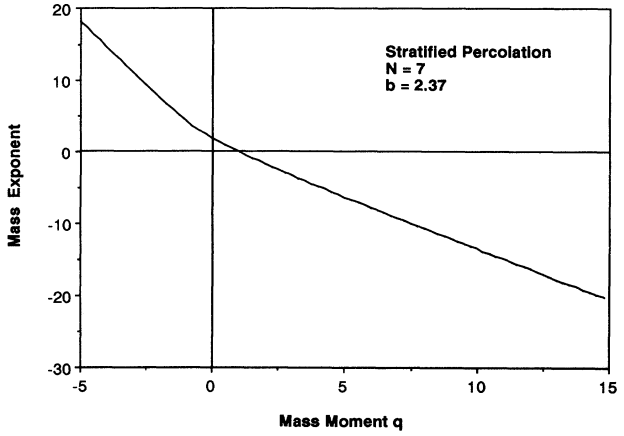

FIG. 12. Mass exponent $\tau(q)$ as a function of mass moment q for a stratified pattern of five tiers with $N=7$ and $b=2.37$.

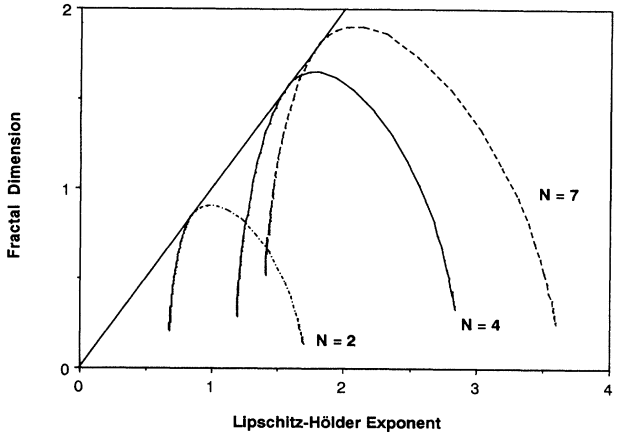

FIG. 14. The $f(\alpha)$ curves for stratified patterns with five tiers and $N=2$, 4, and 7. The curves are all tangent to the line $D=\alpha$. For $N \gg 10$, the curves converge on $D=2$.

Equations (4.9)–(4.12) were applied to stratified percolation simulations. In these calculations, the density of sites described in Sec. III is used to obtain the mass. The mass exponent $\tau(q)$ for a five-tier stratified pattern with $N=7$ and $b=2.37$ is shown in Fig. 12 as a function of mass exponent q. The change in the slope around $q=0$ yields the width of the Lipschitz-Hölder exponent spectrum. This spectrum of exponents α is shown in Fig. 13. The exponents vary between 1 and 4 for this example. Fractal dimensions at $q=0$ define the fractal dimensions of the black region in the black-and-white representations of the patterns.

When the fractal dimensions are plotted as functions of the Lipschitz-Hölder exponents, trends become apparent as the density of sites is increased. The $f(\alpha)$ curves for several patterns are shown in Fig. 14. A purely homogeneous distribution of sites would produce a Kronecker δ at $\alpha=2$. The stratified pattern with $N=7$ has strong correlations and strong inhomogeneities which lead to a wide distribution. The width of the $f(\alpha)$ curve is defined as $\Delta\alpha=\alpha_{\max}-\alpha_{\min}$. The width $\Delta\alpha$ relative to the peak value D is plotted as functions of the total number $M=N^n$ of final squares for three tiers and five tiers in Fig. 15. The ratio $\Delta\alpha/D$ is approximately constant and equal to unity up to 10^5 squares plotted. The origin of this invariance is not understood, but is not a general property of multifractals, and may be peculiar to hierarchical cascades.

V. FINITE-SIZE PERCOLATION PROPERTIES

A fundamental aspect of percolating systems is a dependence of the percolation properties on the size of the system. The percolation formalism was first studied formally by Broadbent and Hammersley [51]. Many reviews cover the earlier history and newest trends in per-

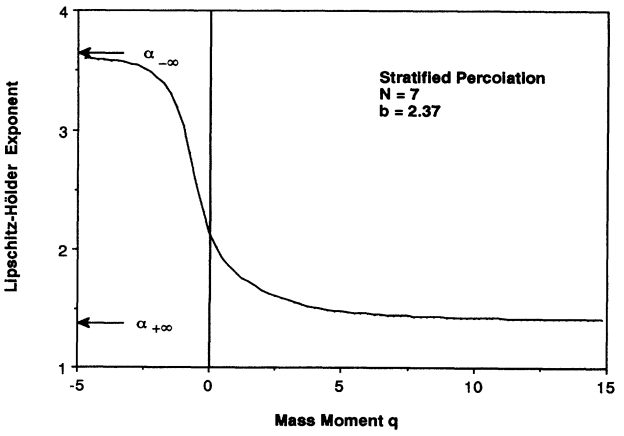

FIG. 13. The Lipschitz-Hölder exponent $\alpha(q)$ as a function of mass moment q for the stratified pattern of Fig. 12. The limits α_∞ and $\alpha_{-\infty}$ are shown for $q\to\infty$ and $q\to-\infty$, respectively.

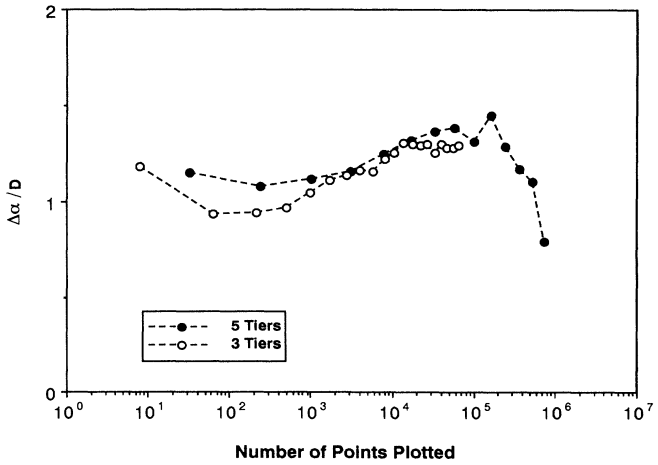

FIG. 15. Width $\Delta\alpha/D$ of the spectrum of $f(\alpha)$ as a function of the total number of points plotted for three and five tiers. The relative width remains approximately equal to unity up to 10^5 points plotted.

colation theory [51–57]. Percolation probabilities are functions of the pattern occupancy p. A central feature of percolation theory is the critical threshold p_c. For infinite systems, when the occupancy is below p_c, then connected paths across the pattern do not occur. For occupancies $p-p_c>0$, a connected path exists, and the pattern is said to percolate. For finite systems, these statements must be modified as described below.

A. Real-space-renormalization group

Percolation is a critical phenomenon. Many of the macroscopic properties of a random system, such as conductivity in a random resistor network, or the order parameter in magnetic systems, are singular at the critical threshold. Of particular interest are the critical exponents, such as β and ν [55]. These exponents often depend only on the dimensionality of the space and help define universality classes. A powerful tool for obtaining these exponents is the renormalization-group theory. Renormalization-group theory was developed to study phase transitions and critical phenomena [58,59], and the theory, in its real-space variant [60], can be naturally applied to percolation problems [61].

Consider, as the renormalization group for percolation, the group of transformations $R(b,p)$ that rescale a selected region of a percolation pattern by a factor of b. After this "renormalization" of the size of the percolation pattern, the effective occupancy of the new pattern has been changed to p' given by

$$p'=R(b,p)\ . \tag{5.1}$$

The concentration p^* for which the transformation $R(b,p^*)$ leaves the occupancy invariant ($p'=p^*=p$) is called the fixed point of the transformation, and may be used to define the critical threshold of the pattern for the renormalization factor b. The single-parameter renormalization transformation Eq. (5.1) is approximately valid when considering a single cell with a size b that is "large" relative to the resolution size of the pattern, and is expected to become exact as the cell size goes to infinity.

A central feature of a real-space renormalization-group theory is the treatment of finite-size cells. The ideas of finite-size scaling [62,63] are closely related to those of the renormalization-group theory [64,65]. At the heart of renormalization is the scaling hypothesis. As applied to finite-size systems, this states that a critical probability that depends on two variables $P(p-p_c,L)$ has the scaling form

$$P=L^{-A}F((p-p_c)L^{B}) \tag{5.2}$$

for $p\to p_c$ and $L\to\infty$. To satisfy the asymptotic relations

$$R=\begin{cases}0 & (p-p_c)<0\\ 1 & (p-p_c)>0\end{cases} \tag{5.3}$$

as the size of the system $L\to\infty$, the finite-size spanning probability becomes [57]

$$R=H((p-p_c)L^{1/\nu})\ , \tag{5.4}$$

where $H(z)$ is a scaling function, with the property that $H(z)\to 1$ as $z\to\infty$ and $H(z)\to 0$ as $z\to-\infty$, that can be obtained from numerical computation. The correlation length ξ (also called the pair-connectedness length) is the average linear separation between positions of a connected finite cluster. The correlation length diverges as $p\to p_c$,

$$\xi\propto(p-p_c)^{-\nu}\ , \tag{5.5}$$

where $\nu=\frac{4}{3}$ is the correlation length exponent for two dimensions. The goal of finite-size scaling is to calculate percolation properties as a function of cell size L, and to extrapolate to the case of $L\to\infty$. The correlation length exponent ν plays a key role for finite-size effects when $L\leq\xi$.

The width σ of the transition can be used to find the correlation exponent ν. Near to the fixed point, the renormalization equation (5.1) can be linearized to

$$(p'-p^*)=\lambda(p-p^*) \tag{5.6}$$

with the eigenvalue λ given by

$$\lambda=\left.\frac{dR}{dp}\right|_{p=p^*}\propto\sigma^{-1} \tag{5.7}$$

which is related to the correlation exponent ν through the derivative of Eq. (5.4) by

$$\sigma^{-1}\propto L^{1/\nu}\ . \tag{5.8}$$

Here, we use the Monte Carlo renormalization group to implement a finite-size scaling calculation of the spanning probability $R(L,p-p_c)$ from which the critical threshold p_c and the critical exponent ν can be obtained.

B. Monte Carlo simulations

To find the probabilities $R(p-p_c,L)$ for a percolation pattern, we start with a 300×300 array of pixels. Onto this array, we plot a percolation pattern of squares. The size of the squares is 4×4 pixels. This square size retains the features of continuum percolation. To check for percolation, the resulting array is viewed as a site percolation problem. Pixels that are black are available; pixels that are white are unavailable. Flow can only occur between two adjacent available pixels. A square cell of side L is said to percolate if a connected path of available sites spans the cell from one side to the opposite side. We check for this connected path for each cell using a cluster numbering algorithm [66]. The tabulation of the number of cells that are spanned yields the spanning probability $R(p-p_c,L)$ for that cell size. We take as our rule for a spanning cluster the condition where the cell is spanned in either the vertical or horizontal direction. This rule [61] is called R_0. The Monte Carlo spanning probabilities for one stratified percolation pattern are obtained from

$$R(L)=\frac{\sum_{i=1}^{k^2}S_i(L)}{k^2} \tag{5.9}$$

where $k=1,2,3,6$ with $L=300/k$. $S_i(L)=1$ if the ith cell percolates, and $S_i(L)=0$ if it does not. The results of many patterns are then averaged to obtain smooth functions for $R(L,p)$.

The spanning probability for Monte Carlo simulations of random (uncorrelated) continuum percolation [represented in Fig. 2(a) with a fractal dimension $D=2.00$] is shown in Fig. 16. The simulations were run on a 300×300 grid with a square size of 4×4 pixels. The percolation threshold is relatively sharp and occurs at $A_c=0.62$. This threshold must be compared with the critical threshold for isotropic continuum percolation. The critical area fraction for isotropic continuum percolation is [67] $A_c=0.68$. Isotropic continuum percolation can be represented by writing circles to the grid as the occupying elements, rather than squares. We chose to use squares, because circles are not well defined on a square grid. The difference in thresholds between circles and squares arises because squares are not isotropic, like circles. Increasing anisotropy of the occupying elements decreases the threshold when the elements are distributed randomly (i.e., when the anisotropic elements still produce isotropic percolation patterns). In addition to this anisotropy, the discreteness of the underlying grid, and the 4×4 pixel size for our squares, reduces the threshold by a few percent from the continuum limit.

The results for continuum percolation can be compared with the probabilities in Fig. 17 computed for Monte Carlo simulations of stratified percolation patterns constructed using three tiers and a scale factor of $b=(300/4)^{1/3}=4.22$ between tiers. The simulations were again performed on a 300×300 grid with a smallest square size of 4×4 pixels. The most dramatic difference between stratified percolation and standard continuum percolation is the width of the transition. The width of the stratified percolation transition is roughly ten times broader than standard continuum percolation. This is an intrinsic feature of stratified percolation. Stratified percolation has structure on all length scales. The long-range structure is generated at the scale of the largest

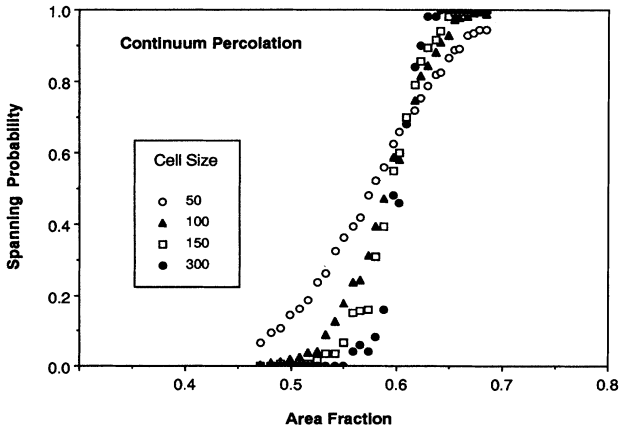

FIG. 16. The spanning probability R vs the covered area for standard continuum percolation using 4×4 squares on a 300×300 lattice for 50 simulations per data point.

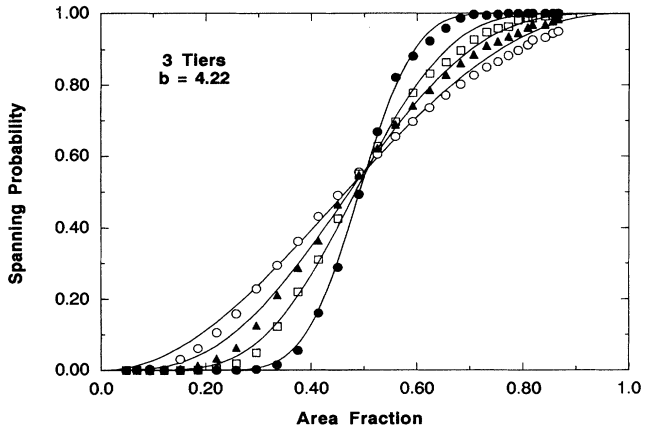

FIG. 17. Spanning probability $R(L,A)$ vs covered area for three-tier stratified patterns. The four cell sizes are $L=50$, 100, 150, and 300. The data are from simulations of 300 patterns per data point, and the solid curves are the fit from the beta functions.

tier. The initial subsquares define large areas of the pattern that will be either dense with sites, or empty. The largest cell size in the renormalization is the same size as the largest tier. The subsquares are smaller by a factor of $b=4.22$. The renormalization of the stratified pattern therefore reflects aspects of renormalization with a small cell of size 4.22. The construction of the stratified pattern forces the renormalization to be intrinsically a small-cell renormalization.

C. Critical percolation properties

To obtain a smoothly varying approximation to the discrete spanning probabilities, the spanning probabilities for stratified percolation in Fig. 17 are fit to a beta distribution. The beta distribution gives better agreement with small-cell renormalization than do Gaussian fits [61]. The smooth fit will allow us to obtain critical thresholds, and inverse widths. The beta distribution is given by

$$B_{nm}(x)=\frac{\Gamma(n+m)}{\Gamma(n)\Gamma(m)}x^{m-1}(1-x)^{n-1},\quad 0\le x\le 1 \tag{5.10}$$

where the mean and the variance of the distribution are given by

$$\langle x\rangle=\frac{m}{m+n},\qquad \sigma^2=\frac{mn}{(m+n)^2(m+n+1)}. \tag{5.11}$$

The spanning probability is fit by integrating the beta distribution

$$R_{nm}(x)=\int_0^x B_{nm}(x)dx \tag{5.12}$$

and adjusting m and n to fit the correct dependence of the simulations near the threshold.

The threshold of a finite system is not uniquely defined. Different criteria used to define the threshold yield

different thresholds. In the face of this ambiguity, one may want to choose a "best" criterion. In fact, any criterion for finding the threshold can be used, as long as the dependence of the threshold on the sample size L is taken into account. From Eq. (5.4) one finds that any finite size threshold $p_c(L)$ will differ from the true threshold p_c (for an infinite sample size) by

$$p_c(L)-p_c \propto L^{-1/\nu} . \tag{5.13}$$

By plotting the finite-size thresholds $p_c(L)$ vs $L^{-1/\nu}$, for different values of ν, a good linear fit can be found. This procedure not only gives a value for the exponent ν, but also yields p_c by extrapolating to $L=\infty$. Any choice of criterion for the thresholds $p_c(L)$ should extrapolate to the same p_c with the same exponent ν.

We choose two different criteria for our thresholds: the fixed points p^*, and the average $p_{av}=\langle x \rangle$. From the resulting fit to the beta distribution, the fixed points p^* and the averages p_{av} are obtained as functions of cell size. The thresholds from this analysis for the Monte Carlo simulations are plotted in Fig. 18 as functions of $L^{-1/\nu}$

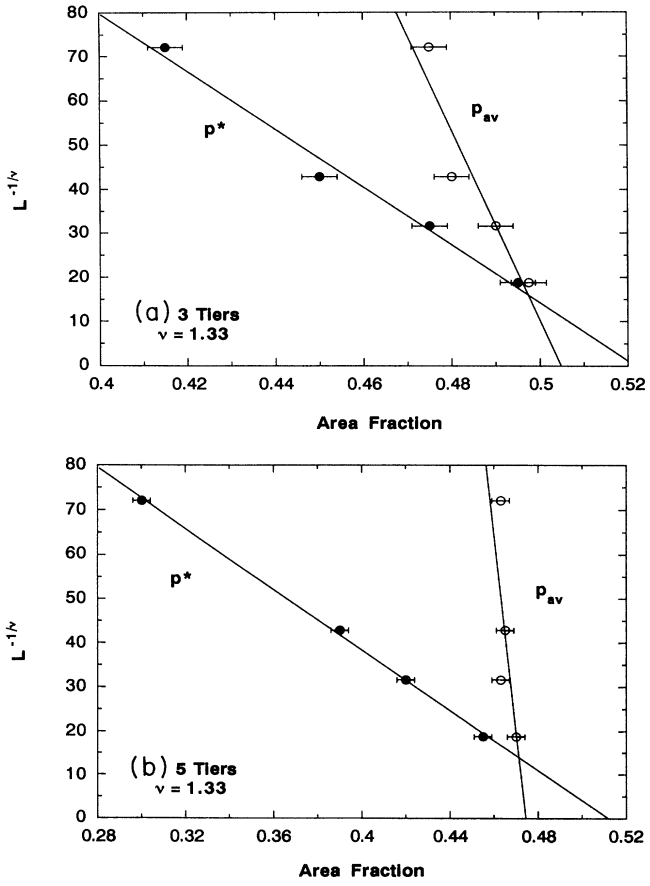

FIG. 18. Threshold values plotted as functions of cell size by fitting the data with beta functions. The fixed points p^* and p_{av} are plotted vs $L^{-1/\nu}$ for (a) three tiers and (b) five tiers. We have chosen a value of $\nu=1.33$ for the analysis. The extrapolation to infinite sample size leads to an ambiguous threshold.

for three tiers and five tiers. A value of $\nu=1.33$ was chosen to check if stratified percolation is consistent with standard percolation. This choice of correlation length exponent does yield linear plots, within the accuracy of the simulations. According to Eq. (5.13), extrapolating to $L\rightarrow\infty$ should lead to the threshold value for an infinite sample size. Furthermore, different criteria for defining the threshold should yield the same p_c. This is not the case in these simulations. The thresholds defined by p^* differ by 4% from the thresholds defined by p_{av}. The reason for this discrepancy may be caused by the small-cell character of stratified percolation. The renormalization procedure is only expected to be valid in the limit of large-cell sizes.

An additional aspect of the critical threshold should be mentioned here. The threshold for an isotropic continuum system without correlations is around 70%. In stratified percolation, the strong correlations (i.e., bunching) have reduced that threshold to around 50%. Other strongly correlated systems have also been shown to have thresholds that approach 50% [10]. In particular, it is interesting to consider that the threshold for Ising correlated percolation is at 50%. While the stratified percolation clusters clearly do not have structures similar to Ising clusters at the critical temperature, they appear to have near symmetry between the black-and-white (up and down) regions. This raises intriguing questions of similarities (and differences) between stratified percolation and other strongly correlated systems.

An alternate critical occupancy can be defined for the stratified patterns. Instead of considering the area fraction of the patterns, we can consider the area fraction per tier $a(N,b)$, given by Eq. (3.3). The area fraction per tier defines how much of the pattern is covered at each tier. From Eq. (3.4), there is a direct one-to-one correspondence between the area fraction $A(N,b)$ and the area fraction per tier $a(N,b)$. The spanning probabilities for three tiers and five tiers are plotted in Fig. 19 against the area fraction per tier and are refit to new beta distributions. The threshold is now close to 70%, which is the canonical value for isotropic continuum percolation. Furthermore, the threshold in the spanning probability is considerably sharper, and appears to be much more like large-cell renormalization (cf. Fig. 16) than small-cell renormalization (cf. Fig. 17). The finite-size extrapolation for the thresholds is shown in Fig. 20 assuming a value of $\nu=1.33$. When plotted against the area fraction per tier, rather than the area fraction, both thresholds p^* and p_{av} extrapolate to the same critical threshold for a given number of tiers, although the fits are worse than in Fig. 18. This is evidence that when the patterns are considered in terms of the area fraction per tier, the renormalization procedure is closer to large-cell renormalization. Therefore the difficulties associated with the intrinsic small-cell properties of stratified percolation can be removed by considering the area fraction per tier.

Rather than assuming a value for ν in Figs. 18 and 20, a value for the correlation exponent ν can be obtained through the inverse of the beta function width σ^{-1} from Eqs. (5.7) and (5.8). The inverse widths are plotted in Fig. 21 versus the cell size L. The inverse width should

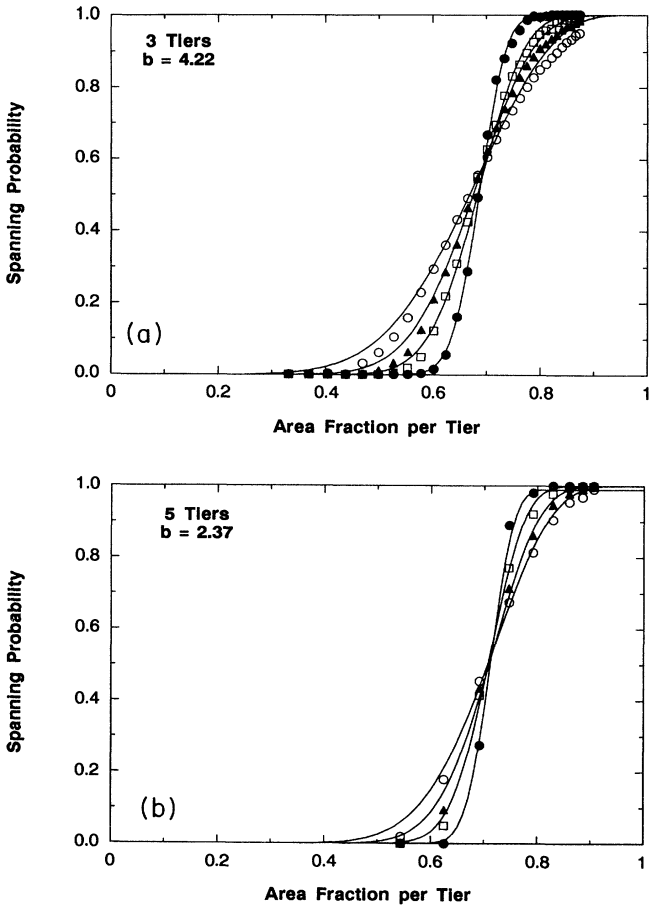

FIG. 19. Spanning probability $R(L,a)$ vs the area fraction per tier for (a) three tiers and (b) five tiers. The sample sizes were $L=50$, 100, 150, and 300. The data are from simulations of 300 patterns per data point and the solid curves are the beta function fits. The thresholds are considerably sharper than in Fig. 17.

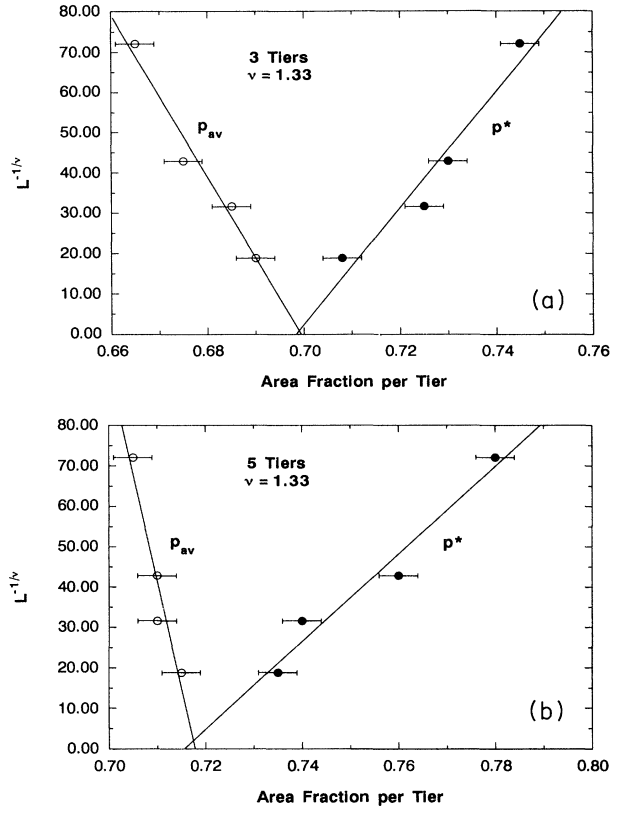

FIG. 20. Threshold values p^* and p_{av} obtained from Fig. 19 for (a) three tiers and (b) five tiers. The extrapolation using $\nu=1.33$ to infinite sample size in each case yields a well-defined threshold: $a_c=0.70$ for three tiers and $a_c=0.72$ for five tiers.

vary as L^{ν} for large L. The straight lines are fit to the values for the three largest L. The resulting correlation exponent is found to be $\nu=1.33\pm0.05$. This value is in good agreement with standard percolation. The strong correlations introduced during the recursive construction do not change the correlation length exponent. This may not be surprising, considering that stratified percolation is constructed of successive layers of standard percolation. Some properties of standard percolation are therefore retained and incorporated in the new stratified percolation.

D. Invariant threshold in stratified percolation

One interesting correspondence between stratified percolation and standard percolation is the critical threshold near 70%, when expressed in terms of the area fraction of a single tier. The strong correlations therefore have also not altered the critical threshold: the threshold of stratified percolation appears to be relatively invariant. However, the origin of this invariance is not obvious. It

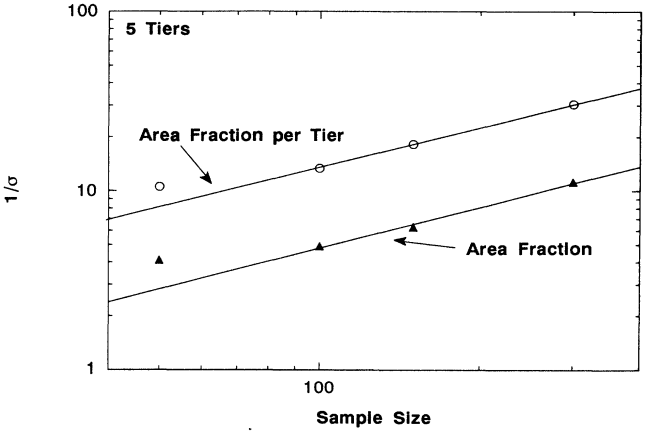

FIG. 21. Inverse width $1/\sigma$ of the transition plotted vs sample size L for five tiers. The widths were obtained from the spanning probabilities $R(L,A)$ and $R(L,a)$, respectively, for the area fraction and the area fraction per tier. The slope of these curves for $L\rightarrow\infty$ yields the exponent $\nu=1.33\pm0.05$.

is caused by the cancellation of two opposite trends: the decrease of the threshold for small-cell sizes; and the increase of the threshold for successively "punctured" tiers.

To demonstrate these two trends, it is simplest to consider the case of two tiers with a scale factor of $b=4.22$, as in Fig. 22(a). On the first tier, the construction is identical to a standard continuum construction. The use of squares (which are anisotropic), and a small cell reduces the threshold from $A_c=0.68$ to $A_c=0.62$. Now consider the effect of replacing each solid square in Fig. 22(a), with a square composed of multiple smaller squares. This is shown in Fig. 22(b). When parts of the original squares are removed, connections that allowed the first pattern to percolate may be broken. To regain percolation, the initial concentration of squares must be increased to compensate for the fact that gaps occur. This increases the area fraction per tier that is necessary for percolation. The critical threshold for five tiers is $a_c=0.717\pm0.002$ (with statistical error only), slightly larger than for three tiers at $a_c=0.700\pm0.002$. Therefore the relatively invariant threshold near 70% may be viewed as a coincidence caused by the cancellation of finite-size effects by the gaps in the subsquares. Despite this coincidence, the near invariance of the threshold for three to five tiers is useful for estimating when this correlated system is near its threshold.

FIG. 22. Finite-size patterns with $N=21$ and $b=4.22$ for (a) one tier, and (b) two tiers. Connections in (a) can fail when the solid squares are replaced by another tier, as in (b). This drives the critical area to larger values for increasing number of tiers. This effect cancels small-cell effects that drive the critical area down, resulting in an approximately invariant threshold for stratified percolation.

VI. CONCLUSIONS

Correlated continuum percolation has a wealth of behavior that makes it a fruitful area to compare against scaling patterns in nature. Many systems in nature show strong correlations in connected continuum systems, such as the flow paths through single fractures in rock. In this paper, we have outlined one correlated continuum percolation model, stratified continuum percolation, that has particularly interesting behavior, is well defined, and may be used to model physical systems. The model is constructed as a self-similar hierarchical cascade with continuous overlap. The cascade generates a multifractal distribution with fractal dimensions that can be continuously tuned by varying the scaling parameter b and the number of squares per level, N. The patterns have percolation thresholds of approximately $A_c\approx0.50$, implying that the strong correlations introduce a symmetry between the covered and uncovered areas. The finite-size scaling properties are intrinsically small cell because of the structure of all length scales. This leads to broad percolation transitions. When the covered area is transformed according to the area fraction per tier, large-cell properties are regained with a threshold near $A_c=0.70$, and with a correlation exponent of $\nu=1.33$.

Stratified percolation is a general construction that should find applications in many situations. The log-normal distribution, due to the random multiplicative processes in the generation, may make it particularly useful for certain situations. Future applications of stratified continuum percolation may include generation and study of hierarchical fracture networks, and invasion percolation into strongly correlated continuum systems. The continuously tunable fractal dimension, while retaining the features of standard percolation, may make this model especially attractive for modeling the fractal geometry of connected patterns generated by critical phenomena.

ACKNOWLEDGMENTS

The authors would like to acknowledge helpful discussions with S. Redner and A. Hirsch, and would like to thank H. Nakanishi for a critical reading of the manuscript. D. D. Nolte would like to thank the Alfred P. Sloan Foundation for support.

[1] D. D. Nolte, L. J. Pyrak-Nolte, and N. G. W. Cook, Pure Appl. Geophys. **131**, 111 (1989).
[2] L. J. Pyrak-Nolte, N. G. W. Cook, and D. D. Nolte, Geophys. Res. Lett. **15**, 1247 (1988).
[3] D. D. Nolte, Phys. Rev. A **40**, 4817 (1989).
[4] H. Müller-Krumbhaar, Phys. Lett. **50A**, 27 (1974).
[5] A. Coniglio, C. R. Nappi, F. Peruggi, and L. Russo, J. Phys. A **10**, 205 (1977).

[1] D. D. Nolte, L. J. Pyrak-Nolte, and N. G. W. Cook, Pure Appl. Geophys. **131**, 111 (1989).
[2] L. J. Pyrak-Nolte, N. G. W. Cook, and D. D. Nolte, Geophys. Res. Lett. **15**, 1247 (1988).
[3] D. D. Nolte, Phys. Rev. A **40**, 4817 (1989).
[4] H. Müller-Krumbhaar, Phys. Lett. **50A**, 27 (1974).
[5] A. Coniglio, C. R. Nappi, F. Peruggi, and L. Russo, J. Phys. A **10**, 205 (1977).
[6] E. Stoll and C. Domb, J. Phys. A **11**, L57 (1978).
[7] A. Coniglio and W. Klein, J. Phys. A **13**, 2775 (1980).
[8] G. F. Tuthill and W. Klein, J. Phys. A **15**, L377 (1982).
[9] A. L. Stella and C. Vanderzands, Phys. Rev. Lett. **62**, 1067 (1989).
[10] L. J. Duckers and R. G. Ross, Phys. Lett. **49A**, 361 (1974).
[11] J. W. Evans, D. R. Burgess, and D. K. Hoffman, J. Chem. Phys. **79**, 5011 (1983).
[12] P. Meakin, J. L. Cardy, E. Loh, and D. J. Scalapino, J. Chem. Phys. **86**, 2380 (1987).
[13] D. E. Sanders and J. W. Evans, Phys. Rev. A **38**, 4186 (1988).
[14] D. S. Gaunt, A. J. Guttmann, and S. G. Whittington, J. Phys. A **12**, 75 (1979).
[15] J. Ketesz, B. K. Chakrabarti, and J. A. M. Duarte, J. Phys. A **15**, L13 (1982).
[16] J. L. Lebowitz and H. Saleur, Physica A **138**, 194 (1986).
[17] B. K. Chakrabarti, K. Kaski, and J. Kertesz, Phys. Lett. **82A**, 97 (1981).
[18] A. E. Gonzalez and P. J. Reynolds, Phys. Lett. **80A**, 357 (1980).
[19] A. Weinrib, Phys. Rev. B **29**, 387 (1984).
[20] J. A. Given, J. Chem. Phys. **90**, 5068 (1989).
[21] T. Vicsek and J. Kertesz, J. Phys. A **14**, L31 (1981).
[22] M. K. Phani and D. Dhar, J. Phys. A **17**, L645 (1984).
[23] B. I. Halperin, S. Feng, and P. N. Sen, Phys. Rev. Lett. **54**, 2391 (1985).
[24] I. Balberg, Philos. Mag. B **56**, 991 (1987).
[25] L. J. Pyrak-Nolte, L. R. Meyer, N. G. W. Cook, and P. A. Witherspoon, in *The 6th International Congress on Rock Mechanics, Proceedings, Vol. 1,* edited by G. Herget and S. Vongpaisal (Balkema, Rotterdam, 1987), p. 225.
[26] A. L. R. Bug, S. A. Safran, G. S. Grest, and I. Webman, Phys. Rev. Lett. **55**, 1896 (1985).
[27] B. B. Mandelbrot, *The Fractal Geometry of Nature* (Freeman, San Francisco, 1982).
[28] C. V. L. Charlier, Ark. Mat. Astron. Fys. **16**, 1 (1922).
[29] F. Hoyle, Astrophys. J. **118**, 513 (1953).
[30] E. A. Novikov and R. W. Stewart, Ist. Ak. Nauk SSR: Ser Geofiz. **3**, 408 (1964).
[31] P. Meakin, A. Coniglio, H. E. Stanley, and T. A. Witten, Phys. Rev. A **34**, 3325 (1986).
[32] P. Meakin, J. Phys. A **21**, 3501 (1988).
[33] L. de Arcangelis, S. Render, and A. Coniglio, Phys. Rev. B **31**, 4725 (1985).
[34] S. Redner, Am. J. Phys. **58**, 267 (1990).
[35] Y. W. Tsang, Water Resour. Res. **20**, 1209 (1984).
[36] J. E. Gale, in *Rock Mechanics: Proceedings of 28th U.S. Symposium,* edited by I. W. Farmer, J. J. K. Daemen, C. S. Desai, C. E. Glass, and S. P. Newman (Balkema, Rotterdam, 1987), p. 1213.
[37] E. Hakami, Ph.D. thesis, Lulea University of Technology, Lulea, Sweden, 1988.
[38] B. Lin and Z. R. Yang, J. Phys. A **19**, L49 (1986).
[39] L. Hao and Z. R. Yang, J. Phys. A **20**, 1627 (1987).
[40] Y. Taguchi, J. Phys. A **20**, 6611 (1987).
[41] B. B. Mandelbrot, J. Fluid Mech. **62**, 331 (1974).
[42] U. Frisch and G. Parisi, Varenna Summer School, edited by Ghil (North-Holland, Amsterdam, 1983), Vol. 88.
[43] P. Grassberger and I. Procaccia, Physica D **13**, 34 (1984).
[44] R. Benzi, G. Paladin, G. Parisi, and A. Vulpiani, J. Phys. A **17**, 3521 (1984).
[45] G. Paladin and A. Vulpiani, Lett. Nuovo Cimento **41**, 1175 (1984).
[46] R. Rammal, C. Tannous, P. Breton, and A.-M. S. Tremblay, Phys. Rev. Lett. **54**, 1718 (1985).
[47] R. Rammal, C. Tannous, and A.-M. S. Tremblay, Phys. Rev. A **31**, 2662 (1985).
[48] L. de Arcangelis, S. Redner, and A. Coniglio, Phys. Rev. B **34**, 4656 (1986).
[49] T. C. Halsey, M. H. Jensen, L. P. Kadanoff, I. Procaccia, and B. I. Shraiman, Phys. Rev. A **33**, 1141 (1986).
[50] C. Armitrano, A. Coniglio, and F. di Liberto, Phys. Rev. Lett. **57**, 1016 (1986).
[51] S. R. Broadbent and J. M. Hammersley, Proc. Cambridge Philos. Soc. **53**, 629 (1957).
[52] K. S. Shante and S. Kirkpartick, Adv. Phys. **20**, 325 (1971).
[53] J. W. Essam, in *Phase Transitions and Critical Phenomena,* edited by C. Domb and M. S. Green (Academic, New York, 1972), Vol. 2, p. 197.
[54] S. Kirkpartick, Rev. Mod. Phys. **45**, 574 (1973).
[55] D. Stauffer, Phys. Rep. **54**, 1 (1978).
[56] J. W. Essam, Rep. Prog. Phys. **43**, 53 (1980).
[57] D. Stauffer, *Introduction to Percolation Theory* (Taylor & Francis, London, 1985).
[58] K. G. Wilson, Rev. Mod. Phys. **47**, 773 (1975).
[59] L. P. Kadanoff, Physics **2**, 263 (1986).
[60] T. W. Burkhardt, in *Real Space Renormalization,* edited by T. W. Burkhardt and J. M. J. VanLeeuwen (Springer-Verlag, Berlin, 1982).
[61] P. J. Reynolds, H. E. Stanley, and W. Klein, Phys. Rev. B **21**, 1223 (1980).
[62] M. E. Fisher, Rep. Prog. Phys. **30**, 615 (1967).
[63] M. E. Fisher, J. Appl. Phys. **38**, 981 (1967).
[64] P. Pfeuty and G. Toulouse, *Introduction to the Renormalization Group and to Critical Phenomena* (Wiley, London 1975).
[65] K. G. Wilson, Sci. Am. **241**, 158 (1979).
[66] J. Hoshen and R. Kopelman, Phys. Rev. B **14**, 3438 (1976).
[67] E. T. Gawlinski and H. E. Stanley, J. Phys. A **14**, L291 (1981).